IEEE Access
Multidisciplinary : Rapid Review : Open Access Journal

Received October 10, 2020, accepted October 31, 2020, date of publication November 9, 2020, date of current version November 19, 2020.

*Digital Object Identifier 10.1109/ACCESS.2020.3036746*

# A Four-Corner-Fed Slotted Waveguide Sparse Array for Near-Field Focusing

**YAXIANG WU[1], (Graduate Student Member, IEEE), BOLIN JIANG[1], MIAO ZHANG[1], (Senior Member, IEEE), JIRO HIROKAWA[2], (Fellow, IEEE), AND QING HUO LIU[3], (Fellow, IEEE)**

[1]Institute of Electromagnetics and Acoustics, Xiamen University, Xiamen 361005, China
[2]Department of Electrical and Electronic Engineering, Tokyo Institute of Technology, Tokyo 152-8552, Japan
[3]Department of Electrical and Computer Engineering, Duke University, Durham, NC 27708, USA

Corresponding author: Miao Zhang (miao@xmu.edu.cn)

This work was supported in part by the National Natural Science Foundation of China under Grant 61971364, and in part by the Fundamental Research Funds for the Central Universities, Xiamen University, under Grant 20720170052.

**ABSTRACT** This article presents a double-layer four-corner-fed slotted waveguide sparse array antenna designed for the near-field-focused applications in the X-band. Generally, it is challenging to realize the ideal phase distribution of the near-field focused array antenna, especially for the near-field focusing array antenna with a focal distance less than 5λ. We propose a four-corner-feed structure associated with appropriate waveguide dimensions to realize approximately ideal phase distribution for a focus at 1.5λ. The sparse array based on the particle swarm optimization is adopted to suppress the sidelobes and the grating lobes on the focal plane caused by the residual phase errors. A test antenna is designed at the center frequency of 10 GHz, and is fabricated by Direct Metal Laser Sintering technique for demonstration. It is verified by the experiment that we achieve satisfying near-field focusing effects, especially in terms of the focal spot size and sidelobe levels on the focal plane 45 mm away from the antenna aperture.

**INDEX TERMS** Slotted waveguide array, sparse array, near-field focusing, short focal distance, tranverse slot, particle swarm optimization, direct metal laser sintering technique.

## I. INTRODUCTION

In recent years, more and more near-field-focused (NFF) antennas have been developed due to their various applications. They are wireless power transfer [1], [2], industrial inspection [3], radio frequency identification (RFID) [4], [5], microwave hyperthermia [6] and radiometric temperature sensor [7]. All of them require high-performance NFF antennas, especially to enhance system efficiency, accuracy, and safety.

Conventional NFF antennas are mainly represented by reflector antennas [8], [9], and dielectric lens antennas [10], [11], where quadratic phase distributions are easy to be implemented. However, the disadvantages of those antennas are apparent as well. They require additional feeds and are difficult to integrate with the systems due to their high profile and large overall size. On the other hand, many research groups have studied NFF planar array antennas based on printed circuit board (PCB) process, such as microstrip patch antennas [3], [5], [7], [12]–[15], microstrip leaky-wave antennas [16], [17], substrate integrated waveguide (SIW) slot antennas [18]–[21], and radial line slot antennas [22], [23]. The key is how to realize the quadratic phase distribution in a NFF planar array. Generally, there were three approaches to achieve the desired phase distribution, i.e., by modulating the length [15] or the width [17], [20] of feedlines, or by changing the positions of radiating elements [16], [20]. The length of the microstrip line between the array elements was tuned to meet the requirement of the excitation phase [15]. However, such an open-edged transmission line had a substantial loss especially at high frequency. The positions of the array elements and the widths of the feedlines were adjusted together to satisfy the phase requirement [20]. Even though no grating lobes were produced duo to a quasi-uniform slot distribution, the phase was sensitive to frequencies. That is, serious deterioration of focusing performance may happen when the frequency changes. On the other hand, it was very convenient to control the phase distribution in coaxial-fed radial line slot antennas [22] by adjusting the positions of radiating elements. Nevertheless, this type of antenna has the inherent problem of polarization control, which usually suffered from high cross-polarization.

The associate editor coordinating the review of this manuscript and approving it for publication was Luyu Zhao.

3-D printing technique is becoming more and more popular in the fields of microwaves and antennas due to its low cost, short processing time, and high manufacturing accuracy [24]–[28]. It is worth noting that applying 3-D printing technique to manufacturing complex antennas even with curved structures may be a suitable choice. However, few scholars have studied NFF antennas based on 3-D printing technique. A backscatter side-channel detection using terahertz near-field focusing was presented in [29], where an NFF antenna was fabricated by the 3-D printing technique. A novel 3-D printed NFF lens antenna operating at 300 GHz was presented in [30]. It transformed the linearly-polarized (LP) incident waves into circularly-polarized (CP) transmitted waves, and further concentrated them at a small spot simultaneously.

Near-field synthesis is also essential for the realization of NFF antennas. For instance, in the application of microwave hyperthermia, high sidelobes may cause damage to healthy tissue around the target. Nevertheless, studies on the near-field synthesis methods are insufficient compared with the far-field ones. It has been proved in [31] that the focal characteristics in the near-field region are similar to those in the far-field one, and the far-field synthesis method can be applied in the near-field application as well. Chebyshev distribution [13], the steepest descent method [32], Bayesian compressive sensing [33], and genetic algorithm [34] have been successfully applied to synthesize the 2-D near-field radiation patterns. Remarkably, an algorithm based on a set of theoretic approach and front-and-back iterative propagation scheme was developed in [23] to shape the focal volume in the near-field region.

As far as we know, the focus's position was generally selected to be at least 3λ away from the antenna aperture [17]. Because the closer the focus is, the more critical phase compensation, which brings a more significant challenge to the feeding network design, is required. However, a closer focus means a higher focusing gain, which can lead to the size reduction in wireless charging and RFID systems and to the enhancement of focusing effects.

In this article, a 3D-printed NFF slotted waveguide array antenna with a focal distance of only 1.5λ is presented, as illustrated in Fig. 1. We propose a four-corner-feed structure to realize the quadratic phase distribution naturally. In this case, the waveguide width can be optimized to achieve the desired phase distribution. In addition, the high sidelobe and the grating lobes on the focal plane, caused by the close focus and the residue phase error, can be eliminated by introducing the sparse array based on the particle swarm optimization. Simulation and measurement results verify that we achieved a desirable focusing effect on the focal plane 45 mm away from the antenna aperture at 10 GHz.

This article is organized as follows. In Sec. II, the performance indices of an NFF antenna, especially in terms of focusing gain, focal shift, depth of focus, and sidelobe level, are investigated in its near-field region. Sec. III introduces the unique four-conner-feed structure for near-filed focusing with a wideband operation. The procedures of array synthesis are described in Sec. IV. The overall antenna design by Ansys HFSS is explained in Sec. V. The details of antenna fabrication and experimental verification are presented in Sec. VI. Section VII summarizes the achievements of this work.

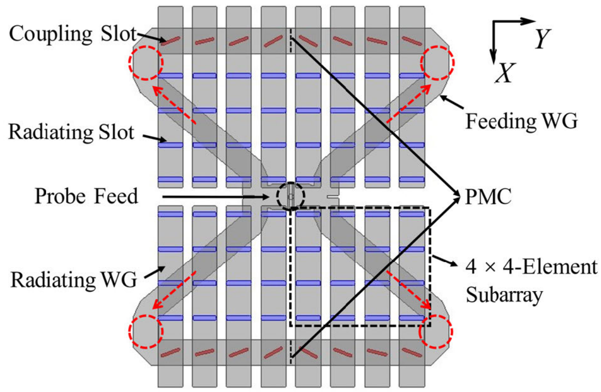


**FIGURE 1.** Configuration of a NFF slotted waveguide antenna with four-corner feed.

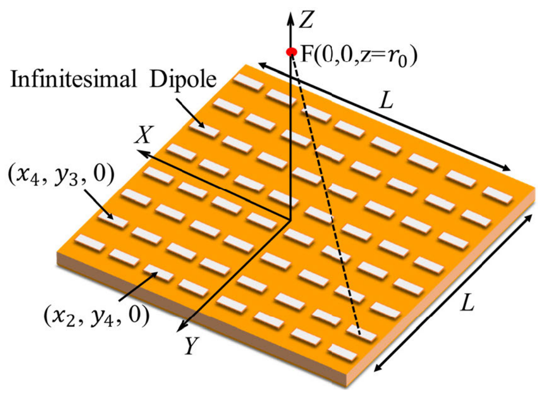


**FIGURE 2.** Analysis model of a dipole array for near-field focusing.

## II. PERFORMANCE INDEX OF AN NFF ARRAY

According to the Babinet's principle and its extension, a dipole is the complementary structure to the slot cut in the waveguide wall. Therefore, an 8 × 8 infinitesimal dipole array in Fig. 2 is adopted to simulate the performance of an 8 × 8-element NFF slotted waveguide array for simplicity. The dipole spacings in both $x$- and $y$-directions are 0.853λ in common at 10 GHz. Those dipoles are assumed to be excited with uniform amplitudes and ideal phases for near-field focusing. The normalized electric field intensities along the $z$-direction are calculated first. As shown in Fig. 3, the $x$-polarized electric field as the co-polarization component almost represents the total electric field intensity [15], while the cross-polarization components are negligible. It should be noted for an NFF array, the following performance indices in terms of focusing gain (FG), focal shift (FS), depth of focus (DoF), sidelobe level (SLL), focal spot size on the focal plane, and axial forelobe level (FLL) [35], [36], are well investigated in this article. Some essential technical terms are explained as follows.

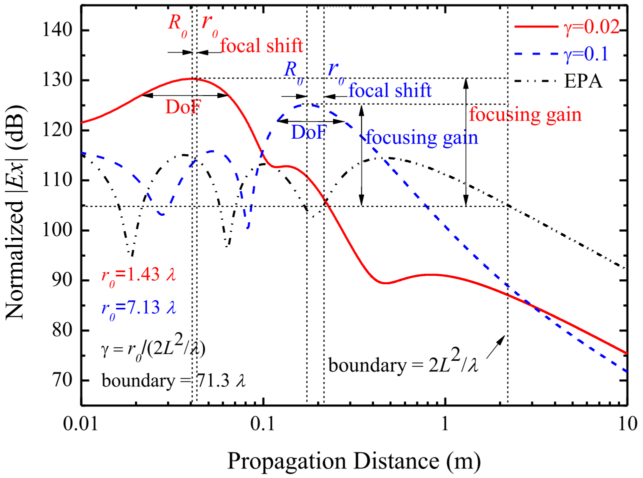


**FIGURE 3.** Normalized electric field intensity $|E_x|$ radiated by an 8 × 8-element NFF array along the $z$-direction at 10 GHz.

The FG is defined as the ratio of an NFF array's peak power density to the power density radiated by the corresponding uniformly-excited array at a distance of $2L^2/\lambda$ in the boresight. Here, $L$ denotes the maximum dimension the array aperture. The FS means the distance between the assigned focal point ($r_0$) and the maximum power density point ($R_0$). The DoF is defined as the distance between two –3-dB axial points around the maximum power density point ($R_0$). The focal spot size is defined as the 3-D region around the focal point where the radiated power density normalized with respect to its maximum value is greater than –3 dB.

As summarized in Fig. 3, the arrays with different values of normalized focal distance (FD), defined as $\gamma = r_0/(2L^2/\lambda)$, behave diversely. It is obvious in Fig. 3, the FG increases and the FS decreases for the shorter focus. Meanwhile, it is worth noting that when the focus lies in the close vicinity of the array aperture, the forelobe disappears.

We further investigate the dependences of FG, FS, DoF, and SLL on the FD within the range of $0 \sim 0.1$ m ($0 \sim 3.3\lambda$ at 10 GHz) in detail. As summarized in Fig. 4, when the focus approaching the array aperture, the FG increases, and the FS, as well as the DoF, decreases. This phenomenon is essential for some near-field applications. On the other hand, the smaller the FD is, the higher the SLL will be, and more phase compensation is required. Therefore, it is very challenging to realize an NFF antenna with a close focus and low sidelobes.

## III. ANTENNA STRUCTURE

To realize a close focus, we introduce a unique four-corner-feed structure [37] instead of the traditional center-feed structure [38] in this article. Fig. 1 illustrates the overall structure of the proposed array antenna. It is composed of two layers: the upper radiating part and the lower feeding part, which is fed by a coaxial probe at the bottom. Through an H-shaped

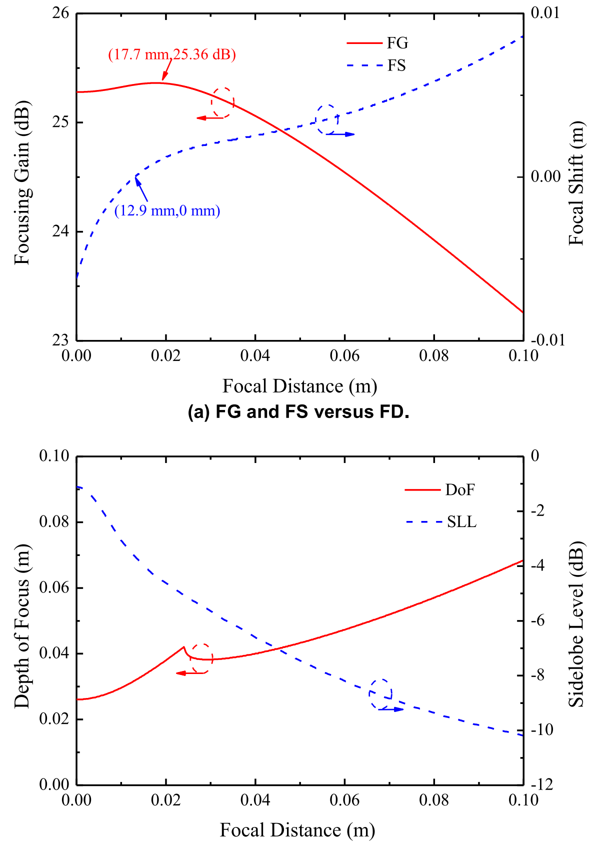


**(a) FG and FS versus FD.**

**(b) DoF and SLL versus FD.**

**FIGURE 4.** FG, FS, DoF and SLL corresponding to FD from 0 m to 0.1 m at 10 GHz. (a) FG and FS versus FD. (b) DoF and SLL versus FD.

power divider, the input power is equally and simultaneously transmitted into four corners without frequency dependence. The design principle of coupling and radiating slots is explained in the following paragraphs.

The center-inclined coupling slots couple the incident wave from the lower feeding waveguide into the upper radiating waveguide. The tilt angle and length of a coupling slot are optimized for tuning the coupling amplitude and phase, respectively. Basically, the spacing between adjacent coupling slots is half guided-wavelength, hence the phase delay for coupling slots fed in-series is multiples of $\pi$. It should be noted that for far-field applications, opposite orientations of adjacent coupling slots have been adopted in [37] to compensate for the alternating phase represented by $n\pi$. On the contrary, the coupling slots in an NFF array orient in the same direction of the waveguide axis. The phase delay occurred inside the feeding waveguide automatically realizes the phase compensation required for near-field focusing. Hence, it is promising to realize an NFF array with wideband characteristics compared to the traditional center-feed structure. Meanwhile, a virtual PMC (Perfect Magnetic Conductor) boundary [39] is generated at the center of a feeding waveguide due to the symmetrical four-corner-feed structure.

Conventionally, the radiation power of a longitudinal slot is mainly controlled by the slot offset [40]. This offset value will change the slot position relative to the focus, which will result in additional large phase error, especially for an NFF array with a close focus. It means the longitudinal slot array is not appropriate for near-field focusing. Uniquely in this study, the transverse slots cut in the broad wall of a hollow waveguide are adopted as the radiating elements, whose spacings are half guided-wavelength in common. The radiation power of a transverse slot [41] is mainly controlled by the slot length and width simultaneously. Hence, the transverse slot is quite suitable for the near-field focusing application since its position remains unchanged when adjusting the excitation amplitude. However, this configuration illustrated in Fig. 2 cannot be adopted in a slotted waveguide array operating in its far-field region, because we have to enlarge the slot spacing from half to one guided-wavelength to ensure the co-phase excitation. Unfortunately, the guided-wavelength in a rectangular waveguide is usually longer than the wavelength in the free space, and leads to the generation of grating lobes. Since the element spacings in both feeding and radiating waveguides are half guided-wavelength in common, the internal phase delays happening in a four-corner-feed structure can be estimated straightforwardly. The values listed in Table 1 are simply the multiples of −180 degrees.

**TABLE 1.** Internal Phase Delays of Actual Array with Four-Corner Feed.

| \|i\|\\\|j\| | 1 | 2 | 3 | 4 |
|---|---|---|---|---|
| 1 | -1080° | -900° | -720° | -540° |
| 2 | -900° | -720° | -540° | -360° |
| 3 | -720° | -540° | -360° | -180° |
| 4 | -540° | -360° | -180° | 0° |

## IV. ARRAY SYNTHESIS

### A. DETERMINATION OF WAVEGUIDE DIMENSIONS

As an example, the proposed antenna illustrated in Fig. 1 is designed at 10 GHz with a focus at $(0, 0, z = r_0)$. It is noteworthy that a focus even with the FD as close as λ/10 can be achieved by adopting the proposed antenna structure. Nevertheless, there is a tradeoff between the FG and the SLL as mentioned above. Therefore, to enhance the FG as well as to suppress the SLL to some extent, we fix $r_0$ at 45 mm (1.5λ) as a more moderate value. In order to focus along the central $z$-axis, the internal phase delay $\varphi_{\text{ij}}$ compensating for the external phase delay should satisfy the following equation with fourfold symmetry.

$$\varphi_{ij} = k\left(\sqrt{x_i^2 + y_j^2 + r_0^2} - \sqrt{x_4^2 + y_4^2 + r_0^2}\right) \tag{1}$$

Here, $i, j$ $(1 \le i, j \le 4)$ are the element number along $x$- and $y$-direction, respectively. $(x_i, y_j)$ is the position of the #$ij$ element. $k$ is the wavenumber in free space at 10 GHz. The guided-wavelength of the $TE_{10}$ mode can be calculated as follows.

$$\lambda_g = \lambda \Big/ \sqrt{1 - (\lambda/2a)} \tag{2}$$

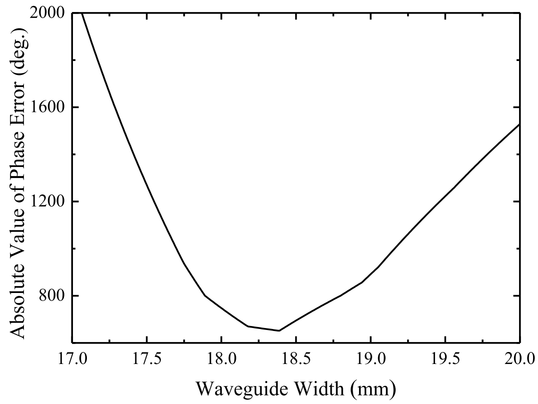


**FIGURE 5.** Sum of the absolute values of phase error as a function of waveguide width *a*.

Here, $a$ is the waveguide width and primarily determines the guided-wavelength. Meanwhile, the parameter $a$ indirectly determines the slot position $(x_i, y_j)$ as well, due to the identical slot spacing of $\lambda_g/2$. As listed in Table 1, the internal phase delay at each slot remains unchanged for different values of $a$. Therefore, the parameter $a$ will be optimized to meet the phase $\varphi_{ij}$ calculated in Eq. (1) for $r_0 = 45$ mm. The phase error is defined as the difference between the actual internal phase delay $(i + j - 8)\pi$ and the ideal phase delay $\varphi_{ij}$. The absolute values of phase errors for all elements are summed up and investigated for different $a$. As shown in Fig. 5, the sum takes the minimum value when $a$ is about 18.4 mm. However, with the consideration of the cutoffs and conductor loss, the final choice of $a$ is 18.5 mm. In this case, the internal ideal phase delays are summarized in Table 2, which are very close to the internal actual phase delays listed in Table 1. The distributions of electric field intensities $|E_x|$ for the NFF arrays with and without phase errors are investigated on the focal plane of $z = 45$ mm. As illustrated in Fig. 6, the actual NFF array with phase errors not only has high sidelobes in both $x$- and $y$-directions, but also has grating lobes in the oblique cut-planes compared with the ideal NFF array without phase errors.

**TABLE 2.** Internal Phase Delays of Ideal Array Focused at 45 mm at 10 GHz.

| \|i\|\\\|j\| | 1 | 2 | 3 | 4 |
|---|---|---|---|---|
| 1 | -1031° | -887° | -662° | -400° |
| 2 | -887° | -767° | -568° | -325° |
| 3 | -662° | -568° | -400° | -186° |
| 4 | -400° | -325° | -186° | 0° |

### B. SUPPRESSION OF SIDELOBES

In order to suppress the sidelobes in the near-field region, we try to adopt the traditional Taylor distribution (SLL = −25 dB, $\bar{n} = 4$), and Gaussian distribution $(\mu = 0, \sigma = 0.5)$ in the NFF array with the actual phase distribution listed in Table 1. The normalized electric field intensities $|E_x|$ along

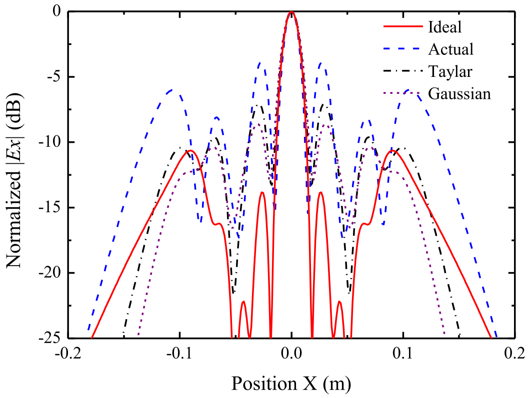


(a) $y = 0$, $z = 45$ mm (*E*-plane).

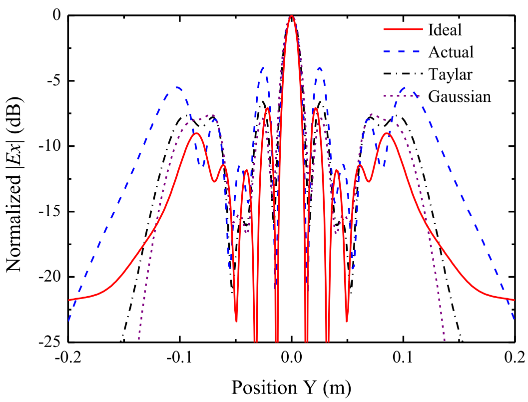


(b) $x = 0$, $z = 45$ mm (*H*-plane).

**FIGURE 6. Calculated normalized electric field intensity $|E_x|$ on the focal plane at 10 GHz. (a) $y = 0$, $z = 45$ mm (*E*-plane). (b) $x = 0$, $z = 45$ mm (*H*-plane).**

the $x$- and $y$-directions on the focal plane at 10 GHz are calculated and summarized in Fig. 6 for comparison. It can be observed from Fig. 6 that the effects of sidelobe suppression due to amplitude tapers are limited at 5 dB and 4 dB along the $x$- and $y$-directions compared with the array with a uniform amplitude excitation.

For further suppression of sidelobes as well as grating lobes on the focal plane, a sparse array based on the particle swarm optimization (PSO) [42] is introduced in our NFF array. Since the spacings of radiating slots associated with the excitation phases are kept unchanged, only their excitation amplitudes are optimized in PSO. During each iteration, only a set of random numbers ranging from 0 to 1, representing the relative excitation amplitude of the radiating slots, is produced by the PSO algorithm. According to the fourfold symmetry, only one-quarter of elements are designed with a remarkable reduction in both computation time and optimization efficiency. The optimized excitation amplitudes of the array elements are summarized in Table 3, where the element with an excitation less than $-15$ dB will be neglected. It is worth noting that even if those elements are ignored, the degradation in SLLs on the focal plane is less than 0.8 dB. In that sense, it leads to a sparse array configuration as listed in Table 4, where the solid circle and the cross represent the existence

**TABLE 3. Optimized Excitation Amplitudes of Array Elements.**

| \|i\|\\\|j\| | 1 | 2 | 3 | 4 |
|---|---|---|---|---|
| 1 | -0.3 dB | -8.5 dB | -9.1 dB | -186.3 dB |
| 2 | -2.0 dB | -192.1 dB | -32.8 dB | -9.2 dB |
| 3 | -2.9 dB | -inf. dB | -185.8 dB | -15.6 dB |
| 4 | -160.1 dB | -7.0 dB | -182.6 dB | -9.6 dB |

and absence of elements, respectively. This sparse array can simplify the design of transverse slots as well. The two-dimensional (2-D) normalized electric field intensities $|E_x|$, the so-called "near-filed radiation patterns" of a sparse array on the focal plane at 10 GHz, are calculated and illustrated in Fig. 7. For simplicity, the one-dimensional (1-D) radiation

**TABLE 4. Sparse Array Configuration.**

| \|i\|\\\|j\| | 1 | 2 | 3 | 4 |
|---|---|---|---|---|
| 1 | ● | ● | ● | × |
| 2 | ● | × | × | ● |
| 3 | ● | × | × | × |
| 4 | × | ● | × | ● |

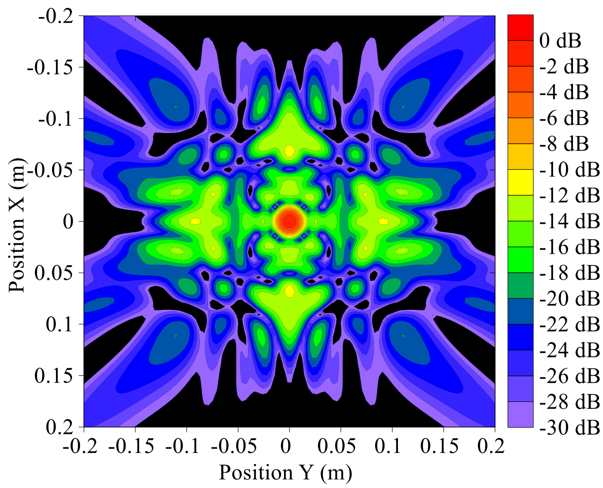


**FIGURE 7. Calculated normalized electric field intensity $|E_x|$ of the sparse array on the focal plane at 10 GHz.**

patterns along the $x$- and $y$-directions are shown in Fig. 8, where the 1-D radiation patterns for the ideal case in Fig. 6 are reproduced for comparison. It is evident in Fig. 8 that the optimized sparse array still has lower sidelobes than the ideal array.

## V. ANTENNA DESIGN

In this article, a high-frequency electromagnetic-field simulator ANSYS HFSS based on the finite element method (FEM), is adopted in the antenna analysis and design. According

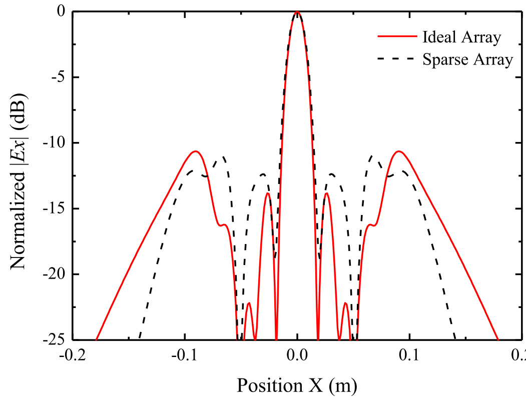

(a) $y = 0$, $z = 45$ mm ($E$-plane).

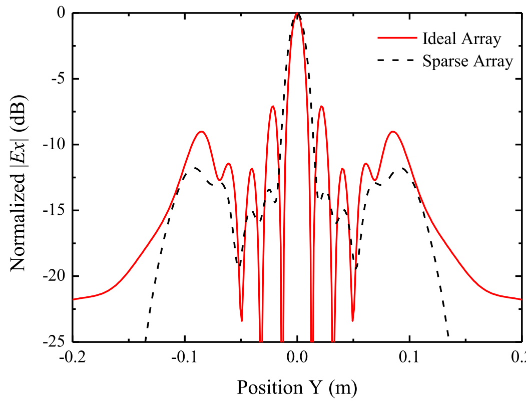

(b) $x = 0$, $z = 45$ mm ($H$-plane).

**FIGURE 8. Calculated normalized electric field intensity $|E_x|$ of the sparse array on the focal plane at 10 GHz. (a) $y = 0$, $z = 45$ mm ($E$-plane). (b) $x = 0$, $z = 45$ mm ($H$-plane).**

to the fourfold symmetry, only the 4 × 4-element radiating subarray, 1×4-element feeding subarray, and primary feeding circuit with cascaded power dividers are to be realized. The design procedures are listed as follows:

*Step 1:* The dimensions of both the feeding and radiating waveguides are determined at 18.5 mm × 9 mm. The thicknesses of both the coupling and radiating slots are selected at 1 mm.

*Step 2:* A SMA probe inserts into the input waveguide. An H-shaped power divider and two kinds of H-plane bends divide the input power into four corners of the lower feeding waveguide with uniform amplitude and phase.

*Step 3:* The inclined angles of coupling slots control the coupling power from the lower feeding waveguide into the upper radiating waveguide. The larger the inclined angle of coupling slots is, the larger the coupling factor is. Meanwhile, the lengths of coupling slots function to compensate for the coupling phase to some extent.

*Step 4:* The subarrays of radiating slots, with different configurations shown in Table 3, need to be designed separately. The lengths and widths of radiating slots are optimized to realize the desired radiating power and to satisfy the matching condition simultaneously. The overall structure of the NFF antenna designed by HFSS is illustrated in Fig. 9.

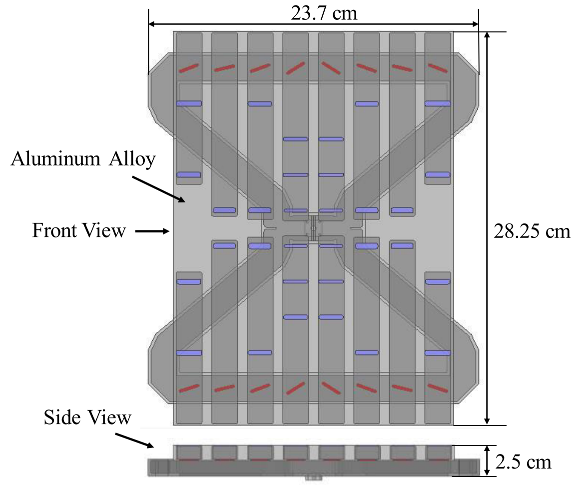


**FIGURE 9. Ovearall structure of the NFF antenna designed by HFSS.**

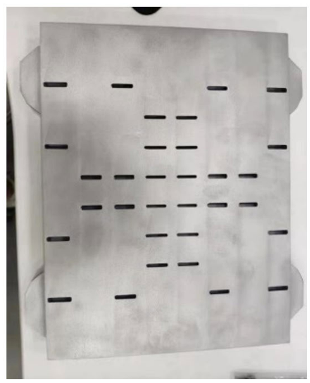

(a) Front side.

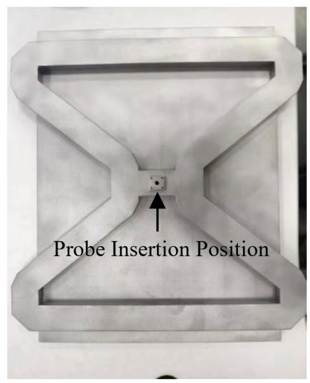


(b) Back side.

**FIGURE 10. Prototype of the proposed NFF antenna. (a) Front side. (b) Back side.**

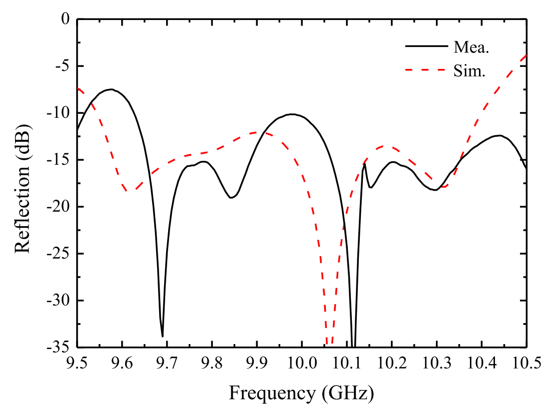


**FIGURE 11. Measured and simulated reflection of the proposed antenna array.**

## VI. ANTENNA FABRICATION AND EVALUATION

The antenna presented in this article is fabricated by a special 3-D printing technique. That is the Direct Metal Laser Sintering of the aluminum alloy powder. The photograph of the prototype antenna is shown in Fig. 10. Its overall dimensions are 282.5 mm × 237 mm × 25 mm.

**FIGURE 12.** Photograph of the near-field measurement environment.

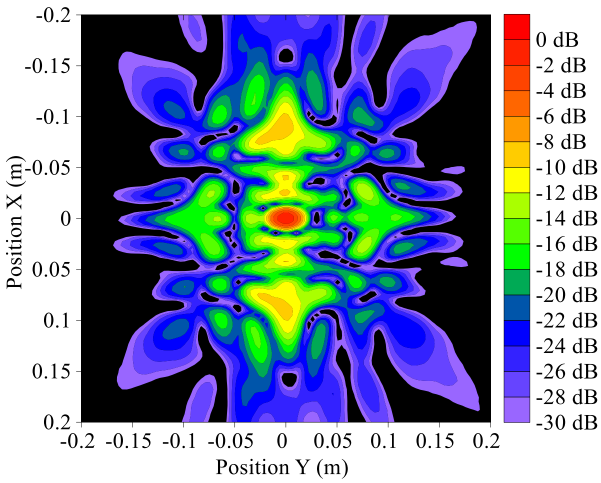


(a) Measured.

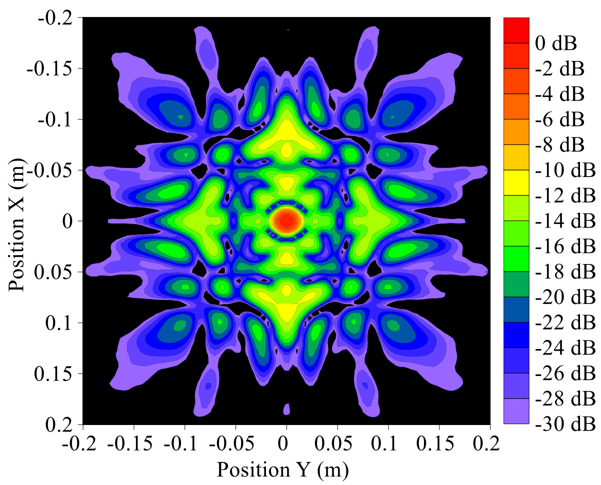


(b) Simulated.

**FIGURE 13.** Measured and simulated normalized electric field intensity $|E_x|$ of the sparse array on the focal plane at 10 GHz. (a) Measured. (b) Simulated.

The reflection of the prototype antenna is measured by using a vector network analyzer. As shown in Fig. 11, the measured and simulated reflections are suppressed below

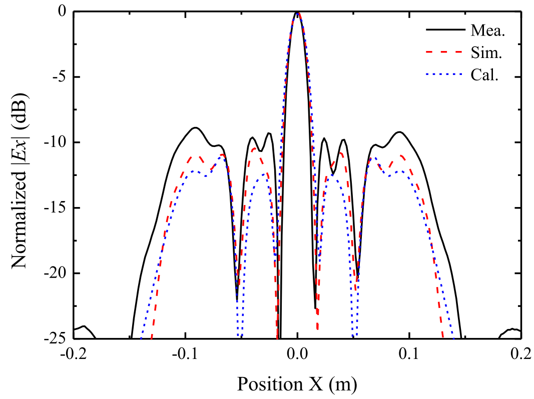


(a) $y = 0$, $z = 45$ mm ($E$-plane).

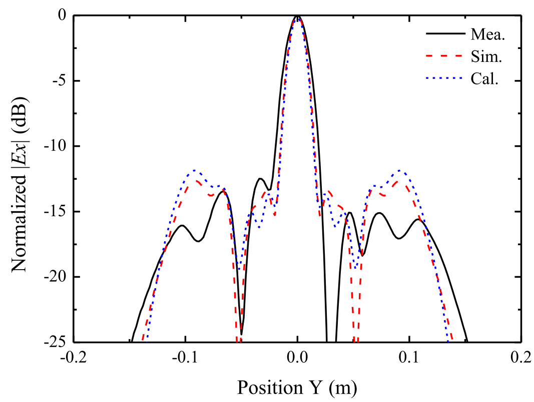


(b) $x = 0$, $z = 45$ mm ($H$-plane).

**FIGURE 14.** Measured, simulated and calculated normalized electric field intensity $|E_X|$ on the focal plane at 10 GHz. (a) $y = 0$, $z = 45$mm ($E$-plane). (b) $x = 0$, $z = 45$mm ($H$-plane).

$-10$ dB over the frequency ranges of 9.63 $\sim$ 10.5 GHz and 9.55 $\sim$ 10.39 GHz, respectively. Even though a small frequency shift is observed, the measured result agrees well with the simulated one. The environment for measuring the electric field in the near-field region is shown in Fig. 12. Under the NSI-MI near-field measurement system, the fabricated antenna is used as the transmitting antenna, and a standard WR-90 open-ended waveguide probe is adopted as the receiving antenna. The measured and simulated electric field intensity $|E_x|$ on the focal plane at 10 GHz are shown in Fig. 13 (a) and (b), respectively. The measured and simulated elliptical areas of the 3-dB focal spot on the focal plane are about 14 mm $\times$ 22 mm and 15.8 mm $\times$ 17.6 mm, respectively. The near-field radiation patterns along the $x$- and $y$-directions on the focal plane at 10 GHz are summarized in Fig. 14, where the results calculated by Matlab are represented and denoted by "Cal.". The test antenna is relatively large and fabricated by Direct Metal Laser Sintering technique as our first attempt. The fabrication error is larger than expected, and the antenna surface is not smooth. These issues lead to the slight asymmetry observed in the measured radiation pattern, as shown in Fig. 13 (a). The SLLs along $x$-direction degrade to $-8.8$ dB, while the SLLs along $y$-direction are well suppressed below $-10$ dB, as respectively illustrated in Fig. 14 (a) and (b).

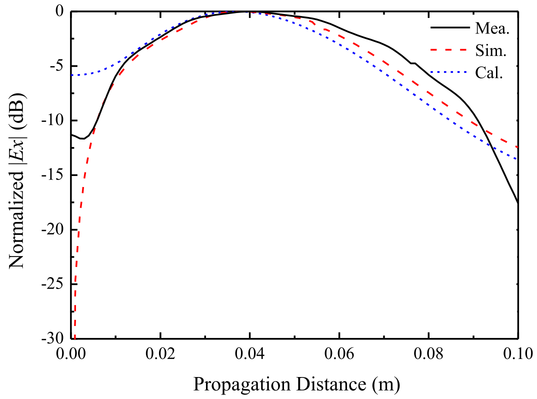


**FIGURE 15.** Measured, simulated and calculated normalized electric field intensity $|E_x|$ of the proposed antenna array along the $z$-axis at 10 GHz.

**TABLE 5.** Performance Comparison Among Various NFF Arrays.

| Ant. | Freq. (GHz) | FD (λ) | DoF (λ) | FS (λ) | SLL (dB) | FLL (dB) |
|---|---|---|---|---|---|---|
| [16] | 15 | 5.5 | 3 | N.A. | -8 | -7 |
| [17] | 15 | 3 | 1.25 | N.A. | -3 | -15 |
| [21] | 35 | 11.7 | N.A. | 1.63 | -17 | -6 |
| This work | 10 | 1.5 | 1.4 | 0.16 | -8.8 | -11 |

The measured, simulated, and calculated normalized electric field intensity $|E_x|$ along the $z$-axis at 10 GHz are summarized in Fig. 15 for comparison. Those results agree well with each other. Meanwhile, the maximum values of the measured, simulated, and calculated curves occur at $z = 40$ mm, 38 mm, and 37 mm, respectively. Table 5 summarizes the performances of various NFF arrays, especially in terms of operating frequency, FD, DoF, FS, SLL and FLL. It is worth noting that the SLL in [21] is measured in the plane where the maximum power density point is located, and the SLLs in other references are measured in their focal planes.

## VII. CONCLUSION

A four-corner-fed slotted waveguide array for near-field focusing is successfully developed in the X-band. This antenna achieves an ultra-close focus with relatively low sidelobes on the focal plane of 45 mm at 10 GHz. The internal dramatic phase delay caused by the four-corner-feed structure can automatically compensate for the external phase delay with broad bandwidth. The waveguide width is optimized to further reduce the phase error. We adopt the transverse radiating slot, which has significant advantages over the longitudinal slot in an NFF array. A sparse array based on particle swarm optimization (PSO) is introduced to realize low SLLs and to eliminate the grating lobes caused by residual phase errors. A prototype antenna is fabricated by the Direct Metal Laser Sintering technique. After a detailed experimental evaluation of reflection, near-field radiating patterns, etc., good agreements are observed in the calculated, simulated, and measured results. On the focal plane of $z = 45$ mm, the sidelobes are suppressed almost below $-10$ dB in all cut-planes. This novel NFF array antenna has good prospects in near-field focusing application that requires an ultra-close focus and relatively low sidelobes.

## ACKNOWLEDGMENT

The authors would like to thank Prof. Guan-Long Huang of Shenzhen University for helping us with the antenna fabrication.

## REFERENCES

[1] S. Kim, J. S. Ho, and A. S. Y. Poon, "Wireless power transfer to miniature implants: Transmitter optimization," *IEEE Trans. Antennas Propag.*, vol. 60, no. 10, pp. 4838–4845, Oct. 2012.

[2] J. O. McSpadden and J. C. Mankins, "Space solar power programs and microwave wireless power transmission technology," *IEEE Microw. Mag.*, vol. 3, no. 4, pp. 46–57, Dec. 2002.

[3] M. Bogosanovic and A. G. Williamson, "Microstrip antenna array with a beam focused in the near-field zone for application in noncontact microwave industrial inspection," *IEEE Trans. Instrum. Meas.*, vol. 56, no. 6, pp. 2186–2195, Dec. 2007.

[4] H.-T. Chou, T.-M. Hung, N.-N. Wang, H.-H. Chou, C. Tung, and P. Nepa, "Design of a near-field focused reflectarray antenna for 2.4 GHz RFID reader applications," *IEEE Trans. Antennas Propag.*, vol. 59, no. 3, pp. 1013–1018, Mar. 2011.

[5] A. Buffi, A. A. Serra, P. Nepa, H.-T. Chou, and G. Manara, "A focused planar microstrip array for 2.4 GHz RFID readers," *IEEE Trans. Antennas Propag.*, vol. 58, no. 5, pp. 1536–1544, May 2010.

[6] D. A. M. Iero, L. Crocco, and T. Isernia, "Thermal and microwave constrained focusing for patient-specific breast cancer hyperthermia: A robustness assessment," *IEEE Trans. Antennas Propag.*, vol. 62, no. 2, pp. 814–821, Feb. 2014.

[7] K. D. Stephan, J. B. Mead, D. M. Pozar, L. Wang, and J. A. Pearce, "A near field focused microstrip array for a radiometric temperature sensor," *IEEE Trans. Antennas Propag.*, vol. 55, no. 4, pp. 1199–1203, Apr. 2007.

[8] D. Cheng and S. Moseley, "On-axis defocus characteristics of the paraboloidal reflector," *IRE Trans. Antennas Propag.*, vol. 3, no. 4, pp. 214–216, Oct. 1955.

[9] L. Shafai, A. A. Kishk, and A. Sebak, "Near field focusing of apertures and reflector antennas," in *Proc. WESCANEX, Commun., Power Comput. Conf.*, May 1997, pp. 246–251.

[10] S. Karimkashi and A. A. Kishk, "Focusing properties of Fresnel zone plate lens antennas in the near-field region," *IEEE Trans. Antennas Propag.*, vol. 59, no. 5, pp. 1481–1487, May 2011.

[11] R. Shavit, T. Wells, and A. Cohen, "Forward-scattering analysis in a focused-beam system," *IEEE Trans. Antennas Propag.*, vol. 46, no. 4, pp. 563–569, Apr. 1998.

[12] F. Tofigh, J. Nourinia, M. Azarmanesh, and K. M. Khazaei, "Near-field focused array microstrip planar antenna for medical applications," *IEEE Antennas Wireless Propag. Lett.*, vol. 13, pp. 951–954, 2014.

[13] S. Karimkashi and A. A. Kishk, "Focused microstrip array antenna using a Dolph-Chebyshev near-field design," *IEEE Trans. Antennas Propag.*, vol. 57, no. 12, pp. 3813–3820, Dec. 2009.

[14] L. Shan and W. Geyi, "Optimal design of focused antenna arrays," *IEEE Trans. Antennas Propag.*, vol. 62, no. 11, pp. 5565–5571, Nov. 2014.

[15] P.-F. Li, S.-W. Qu, S. Yang, Y. Liu, and Q. Xue, "Near-field focused array antenna with frequency-tunable focal distance," *IEEE Trans. Antennas Propag.*, vol. 66, no. 7, pp. 3401–3410, Jul. 2018.

[16] A. J. Martinez-Ros, J. L. Gomez-Tornero, V. Losada, F. Mesa, and F. Medina, "Non-uniform sinusoidally modulated half-mode leaky-wave lines for near-field focusing pattern synthesis," *IEEE Trans. Antennas Propag.*, vol. 63, no. 3, pp. 1022–1031, Mar. 2015.

[17] A. J. Martinez-Ros, J. L. Gomez-Tornero, F. J. Clemente-Fernandez, and J. Monzo-Cabrera, "Microwave near-field focusing properties of width-tapered microstrip leaky-wave antenna," *IEEE Trans. Antennas Propag.*, vol. 61, no. 6, pp. 2981–2990, Jun. 2013.

[18] Y. F. Wu, Y. J. Cheng, and Z. X. Huang, "Ka-band near-field-focused 2-D steering antenna array with a focused Rotman lens," *IEEE Trans. Antennas Propag.*, vol. 66, no. 10, pp. 5204–5213, Oct. 2018.

[19] Y. F. Wu and Y. J. Cheng, "Proactive conformal antenna array for near-field beam focusing and steering based on curved substrate integrated waveguide," *IEEE Trans. Antennas Propag.*, vol. 67, no. 4, pp. 2354–2363, Apr. 2019.

[20] Y. F. Wu and Y. J. Cheng, "Two-dimensional near-field focusing folded reversely fed leaky-wave antenna array with high radiation efficiency," *IEEE Trans. Antennas Propag.*, vol. 67, no. 7, pp. 4560–4569, Jul. 2019.

[21] Y. J. Cheng and F. Xue, "Ka-band near-field-focused array antenna with variable focal point," *IEEE Trans. Antennas Propag.*, vol. 64, no. 5, pp. 1725–1732, May 2016.

[22] M. Ettorre, M. Casaletti, G. Valerio, R. Sauleau, L. L. Coq, S. C. Pavone, and M. Albani, "On the near-field shaping and focusing capability of a radial line slot array," *IEEE Trans. Antennas Propag.*, vol. 62, no. 4, pp. 1991–1999, Apr. 2014.

[23] I. Iliopoulos, M. Casaletti, R. Sauleau, P. Pouliguen, P. Potier, and M. Ettorre, "3-D shaping of a focused aperture in the near field," *IEEE Trans. Antennas Propag.*, vol. 64, no. 12, pp. 5262–5271, Dec. 2016.

[24] M. D'Auria, W. J. Otter, J. Hazell, B. T. W. Gillatt, C. Long-Collins, N. M. Ridler, and S. Lucyszyn, "3-D printed metal-pipe rectangular waveguides," *IEEE Trans. Compon., Packag., Manuf. Technol.*, vol. 5, no. 9, pp. 1339–1349, Sep. 2015.

[25] G. P. Le Sage, "3D printed waveguide slot array antennas," *IEEE Access*, vol. 4, pp. 1258–1265, Mar. 2016.

[26] S.-G. Zhou, G.-L. Huang, and T.-H. Chio, "A lightweight, wideband, dual-circular-polarized waveguide cavity array designed with direct metal laser sintering considerations," *IEEE Trans. Antennas Propag.*, vol. 66, no. 2, pp. 675–682, Feb. 2018.

[27] G.-L. Huang, S.-G. Zhou, T.-H. Chio, and T.-S. Yeo, "Fabrication of a high-efficiency waveguide antenna array via direct metal laser sintering," *IEEE Antennas Wireless Propag. Lett.*, vol. 15, pp. 622–625, 2016.

[28] G.-L. Huang, S.-G. Zhou, T.-H. Chio, C.-Y.-D. Sim, and T.-S. Yeo, "Wide-band dual-polarized and dual-monopulse compact array for SAR system integration applications," *IEEE Geosci. Remote Sens. Lett.*, vol. 13, no. 8, pp. 1203–1207, Aug. 2016.

[29] S. Adibelli, P. Juyal, C.-L. Cheng, and A. Zajic, "Terahertz near-field focusing using a 3-D printed Cassegrain configuration for backscattered side-channel detection," *IEEE Trans. Antennas Propag.*, vol. 67, no. 10, pp. 6627–6638, Oct. 2019.

[30] G. Wu, Y. Zeng, K. F. Chan, S. Qu, and C. H. Chan, "3-D printed terahertz lens with circularly polarized focused near field," in *Proc. 13th Eur. Conf. Antennas Propag. (EuCAP)*, Mar. 2019, pp. 1–4.

[31] R. Hansen, "Focal region characteristics of focused array antennas," *IEEE Trans. Antennas Propag.*, vol. AP-33, no. 12, pp. 1328–1337, Dec. 1985.

[32] H.-T. Chou, K.-L. Hung, and H.-H. Chou, "Design of periodic antenna arrays with the excitation phases synthesized for optimum near-field patterns via steepest descent method," *IEEE Trans. Antennas Propag.*, vol. 59, no. 11, pp. 4342–4345, Nov. 2011.

[33] Z. X. Huang and Y. J. Cheng, "Near-field pattern synthesis for sparse focusing antenna arrays based on Bayesian compressive sensing and convex optimization," *IEEE Trans. Antennas Propag.*, vol. 66, no. 10, pp. 5249–5257, Oct. 2018.

[34] S. Clauzier, S. M. Mikki, and Y. M. M. Antar, "Design of near-field synthesis arrays through global optimization," *IEEE Trans. Antennas Propag.*, vol. 63, no. 1, pp. 151–165, Jan. 2015.

[35] P. Nepa and A. Buffi, "Near-field-focused microwave antennas: Near-field shaping and implementation," *IEEE Antennas Propag. Mag.*, vol. 59, no. 3, pp. 42–53, Jun. 2017.

[36] A. Buffi, P. Nepa, and G. Manara, "Design criteria for near-field-focused planar arrays," *IEEE Antennas Propag. Mag.*, vol. 54, no. 1, pp. 40–50, Feb. 2012.

[37] M. Zhang, J. Hirokawa, and M. Ando, "A four-corner-fed double-layer waveguide slot array with low sidelobes developed for a 40 GHz-band DDD system," *IEEE Trans. Antennas Propag.*, vol. 64, no. 5, pp. 2005–2010, May 2016.

[38] S. Park, Y. Tsunemitsu, J. Hirokawa, and M. Ando, "Center feed single layer slotted waveguide array," *IEEE Trans. Antennas Propag.*, vol. 54, no. 5, pp. 1474–1480, May 2006.

[39] M. Zhang, J. Hirokawa, and M. Ando, "An E-band partially corporate feed uniform slot array with laminated quasi double-layer waveguide and virtual PMC terminations," *IEEE Trans. Antennas Propag.*, vol. 59, no. 5, pp. 1521–1527, May 2011.

[40] M. Zhang, J. Hirokawa, and M. Ando, "A four-way divider for partially-corporate feed in an alternating-phase fed single-layer slotted waveguide array," *IEEE Trans. Antennas Propag.*, vol. 56, no. 6, pp. 1790–1794, Jun. 2008.

[41] J. Liu, D. R. Jackson, and Y. Long, "Substrate integrated waveguide (SIW) leaky-wave antenna with transverse slots," *IEEE Trans. Antennas Propag.*, vol. 60, no. 1, pp. 20–29, Jan. 2012.

[42] J. Robinson and Y. Rahmat-Samii, "Particle swarm optimization in electromagnetics," *IEEE Trans. Antennas Propag.*, vol. 52, no. 2, pp. 397–407, Feb. 2004.

**YAXIANG WU** (Graduate Student Member, IEEE) received the B.S. degree in electronics and information engineering from Huaibei Normal University, Huaibei, China, in 2018. He is currently pursuing the master's degree with the Institute of Electromagnetics and Acoustics, Xiamen University, Xiamen, China. His current research interests include waveguide slot arrays and high-performance terahertz antennas.

**BOLIN JIANG** received the B.S. degree in electronics and information engineering from Soochow University, Suzhou, China, in 2015, and the M.S. degree in electronics and communications engineering from Xiamen University, Xiamen, China, in 2018. His research interests include antenna arrays and waveguide slot antennas.

**MIAO ZHANG** (Senior Member, IEEE) received the B.S., M.S., and D.E. degrees in electrical and electronic engineering from the Tokyo Institute of Technology, Tokyo, Japan, in 2003, 2005, and 2008, respectively.

From 2005 to 2008, he was a Research Fellow of the Japan Society for the Promotion of Science, Tokyo. Since 2008, he has been a Researcher with the Tokyo Institute of Technology, where he became an Assistant Professor in 2013. He is currently an Associate Professor with Xiamen University, Fujian, China. His research interests include waveguide slot arrays, millimeter-wave antennas, and array antennas for 5G and car-radar applications. He is a Senior Member of CIE and IEICE. He was a recipient of the Best Letter Award, in 2009, from the IEICE Communication Society, the Young Engineer Award, in 2010, from IEICE Technical Committee on Antennas and Propagation, the IEEE AP-S Japan Chapter Young Engineer Award, in 2011, and the Best Paper Award at the 9th European Conference on Antennas and Propagations, in 2015.

**JIRO HIROKAWA** (Fellow, IEEE) received the B.S., M.S., and D.E. degrees in electrical and electronic engineering from the Tokyo Institute of Technology (Tokyo Tech), Tokyo, Japan, in 1988, 1990, and 1994, respectively.

From 1990 to 1996, he was a Research Associate with Tokyo Tech, where he was also an Associate Professor from 1996 to 2015. From 1994 to 1995, he was a Postdoctoral Fellow with the Antenna Group, Chalmers University of Technology, Gothenburg, Sweden. He is currently a Professor with Tokyo Tech. His research interests include slotted waveguide array antennas and millimeter-wave antennas. He is a Fellow of IEICE. He received the IEEE AP-S Tokyo Chapter Young Engineer Award, in 1991, the Young Engineer Award from IEICE, in 1996, the Tokyo Tech Award for Challenging Research, in 2003, the Young Scientists' Prize from the Minister of Education, Culture, Sports, Science and Technology, Japan, in 2005, the Best Paper Award, in 2007, the Best Letter Award from the IEICE Communications Society, in 2009, and the IEICE Best Paper Award, in 2016 and 2018.

**QING HUO LIU** (Fellow, IEEE) received the B.S. and M.S. degrees in physics from Xiamen University, Xiamen, China, and the Ph.D. degree in electrical engineering from the University of Illinois at Urbana–Champaign, Champaign, IL, USA.

From September 1986 to December 1988, he was a Research Assistant with the Electromagnetics Laboratory, University of Illinois at Urbana–Champaign, where he was a Postdoctoral Research Associate from January 1989 to February 1990. He was a Research Scientist and the Program Leader with Schlumberger-Doll Research, Ridgefield, CT, USA, from 1990 to 1995. From 1996 to May 1999, he was an Associate Professor with New Mexico State University, Las Cruces, NM, USA. Since June 1999, he has been with Duke University, Durham, NC, USA, where he is currently a Professor of electrical and computer engineering. He has been also the Founder and the Chairman of Wave Computation Technologies, Inc., since 2005. His research interests include computational electromagnetics and acoustics, inverse problems, and their application in nanophotonics, geophysics, biomedical imaging, and electronic packaging. He has published widely in these areas.

Dr. Liu is a Fellow of the Acoustical Society of America, Electromagnetics Academy, and the Optical Society of America. He received the 1996 Presidential Early Career Award for Scientists and Engineers (PECASE) from the White House, the 1996 Early Career Research Award from the Environmental Protection Agency, the 1997 CAREER Award from the National Science Foundation, the 2017 Technical Achievement Award, the 2018 Computational Electromagnetics Award from the Applied Computational Electromagnetics Society, the 2018 Harrington-Mittra Award in Computational Electromagnetics from the IEEE Antennas and Propagation Society, and the ECE Distinguished Alumni Award from the University of Illinois at Urbana–Champaign in 2018. He served as the Founding Editor-in-Chief for the IEEE Journal on Multiscale and Multiphysics Computational Techniques. He has served as an IEEE Antennas and Propagation Society Distinguished Lecturer.